

Pseudo-View Enhancement via Confidence Fusion for Unposed Sparse-View Reconstruction

Beizhen Zhao^{1*} Sicheng Yu^{1*} Guanzhi Ding¹ Yu Hu¹ Hao Wang^{1†}

¹The Hong Kong University of Science and Technology (Guangzhou)

bzhao610@connect.hkust-gz.edu.cn syu605@connect.hkust-gz.edu.cn haowang@hkust-gz.edu.cn

*Equal Contribution

†Corresponding Author

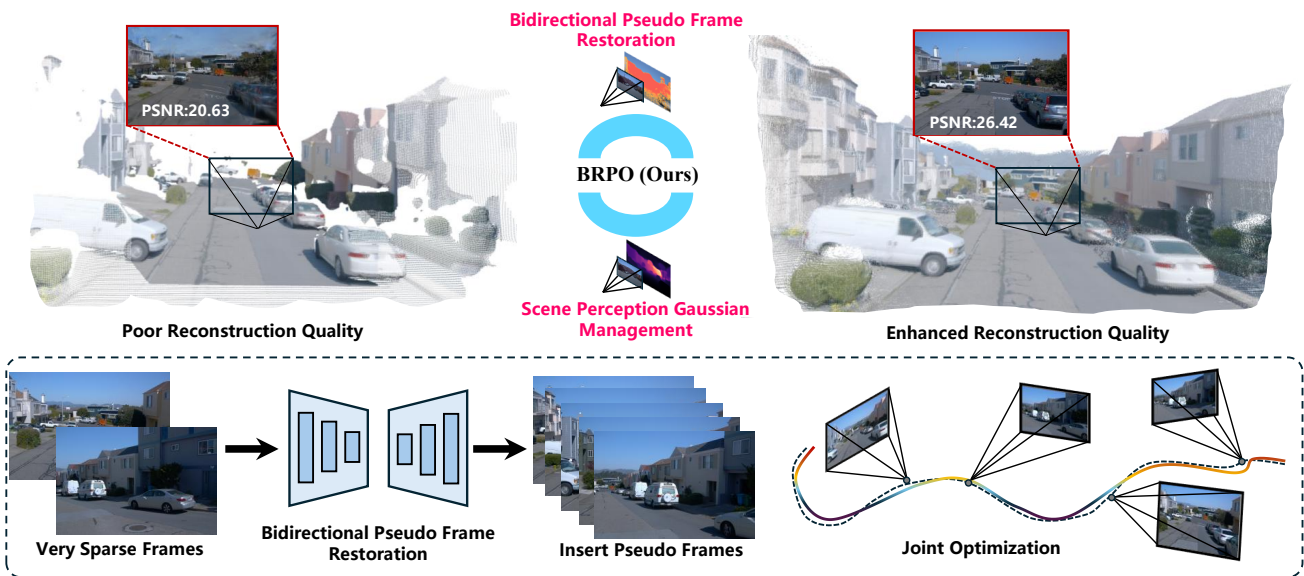


Figure 1. Overview of our pipeline for 3D Gaussian Splatting from unposed sparse views in outdoor scenes. We utilize a cross-view inconsistency UNet and a diffusion model for pseudo view completion. Through a confidence mask and scene perception Gaussian optimization, our method outperforms others in reconstruction quality.

Abstract

3D scene reconstruction under unposed sparse viewpoints is a highly challenging yet practically important problem, especially in outdoor scenes due to complex lighting and scale variation. With extremely limited input views, directly utilizing diffusion model to synthesize pseudo frames will introduce unreasonable geometry, which will harm the final reconstruction quality. To address these issues, we propose a novel framework for sparse-view outdoor reconstruction that achieves high-quality results through bidirectional pseudo frame restoration and scene perception Gaussian management. Specifically, we introduce a bidirectional pseudo frame restoration method that restores missing content by diffusion-based synthesis guided by adjacent

frames with a lightweight pseudo-view deblur model and confidence mask inference algorithm. Then we propose a scene perception Gaussian management strategy that optimize Gaussians based on joint depth-density information. These designs significantly enhance reconstruction completeness, suppress floating artifacts and improve overall geometric consistency under extreme view sparsity. Experiments on outdoor benchmarks demonstrate substantial gains over existing methods in both fidelity and stability.

1. Introduction

Large-scale 3D outdoor scenes reconstruction from unposed and extremely sparse views is of paramount impor-

tance for numerous real-world applications, including autonomous driving, augmented reality, and digital twin systems, which require precise geometry and appearance for robust long-term localization and environment understanding [13, 16, 19, 35]. Consequently, developing a method that can achieve reliable, high-fidelity reconstruction from unposed sparse captures in complex outdoor environments remains a fundamental and significant challenge [38, 41].

3D Gaussian Splatting (3DGS) reconstruction from unposed, sparse-view inputs provides impressive progress for its real-time rendering speed and quality. Despite recent research, existing methods struggle significantly under these conditions. Unposed 3DGS approaches [9, 12, 27] often fail due to insufficient overlap for robust correspondence alignment. Concurrently, methods incorporating geometric priors [15, 32, 38] or recent registration techniques [2, 24] are often limited to refining observed regions or small-scale indoor scenes, failing to recover unobserved geometry in large outdoor environments. Furthermore, generative regularization methods [19, 31, 36] typically presuppose known camera poses or object-centric data, rendering them inapplicable to this challenging unposed, large-scale setting.

To make up the severe lack of multi-view constraints in sparse-view reconstruction, a natural approach is to leverage generative models, such as diffusion, to synthesize pseudo-views and densify the input. However, we find that a diffusion-based completion model usually generates clear but actually unreasonable pseudo-view, which will harm the final reconstruction quality. These plausible-looking but geometrically inconsistent syntheses introduce conflicting information during optimization, leading to artifacts and geometry degradation rather than improvement. Therefore, how to generate reliable and geometrically-consistent pseudo-views remains a critical bottleneck for advancing sparse-view 3D reconstruction.

To address these challenges, we propose a new unposed sparse-view reconstruction framework that focuses on outdoor view restoration Gaussian management. Our key idea is a bidirectional pseudo frame restoration method that enriches visual information for under-constrained regions. To achieve more realistic pseudo view, we first propose a lightweight pseudo-view deblur model for more robust geometric consistency and reliable pseudo frame restoration. Then, instead of blindly using pseudo frames, we design an overlap score fusion and confidence mask inference algorithm that fuse bidirectional pseudo frames based on the viewpoint change and overlap ratio with neighboring inputs and dynamically decides the confidence of pseudo frame through feature mapping and reprojection.

While pseudo-view synthesis effectively improves reconstruction completeness, the sparse input view can cause uneven Gaussians distribution and the difficulty of joint optimization. To overcome this issue, we introduce a scene

perception mechanism that adaptively optimize Gaussians based on perceptual significance. The mechanism leverages an entropy-based depth-density measure to estimate the importance of each Gaussian in representing the local structure, thereby enhancing under-optimized regions.

In summary, our main contributions are as follows:

- A bidirectional pseudo frame restoration method with a pseudo-view deblur network to enhance pseudo view completion.
- An overlap score fusion with confidence mask inference algorithm that selectively synthesizes confidence mask for sparse-view reconstruction.
- A scene perception Gaussian management strategy that adaptively optimize floating Gaussians through depth and density control metric.

Extensive experiments demonstrate that our method substantially outperforms existing 3DGS approaches in reconstruction accuracy, completeness, and visual consistency, offering a new solution for high-quality outdoor 3D reconstruction under sparse-view conditions.

2. Related Work

2.1. Unposed 3D Gaussian splatting

3DGS [13] delivers real-time and high-fidelity novel view synthesis from explicit Gaussians. Yet reconstruction typically relies on COLMAP [26] poses and sparse points, prompting interest in unposed 3DGS, which builds Gaussian scenes directly from raw images.

CF-3DGS [9] initializes the Gaussian field using monocular depth and progressively refines both the camera parameters and Gaussians during optimization. COGS [12] performs incremental scene reconstruction by aligning cameras through dense 2D correspondences, while Rob-GS [7] introduces a robust pairwise registration strategy to stabilize pose estimation. Several methods [7, 12, 27] recover camera geometry through dense 2D correspondence alignment, pairwise registration, or joint optimization, thereby enabling incremental, calibration-free reconstruction. In parallel, a series of 3DGS-SLAM frameworks [4, 21, 25, 35] achieve unposed reconstruction by streaming images as input. Recent works leverage pretrained geometric models to improve unposed 3DGS. InstantSplat [8] employs DUST3R [30] for initialization and accelerates convergence through parallel grid partitioning, though its scalability remains limited under sparse-view inputs. LongSplat [16] integrates MAST3R [14] priors with incremental joint optimization and an efficient octree anchor mechanism, supporting long sequences for novel view synthesis. [3] utilize sub-graph alignment and joint optimization based on VGGT [29] to extend reconstruction to outdoor long sequences.

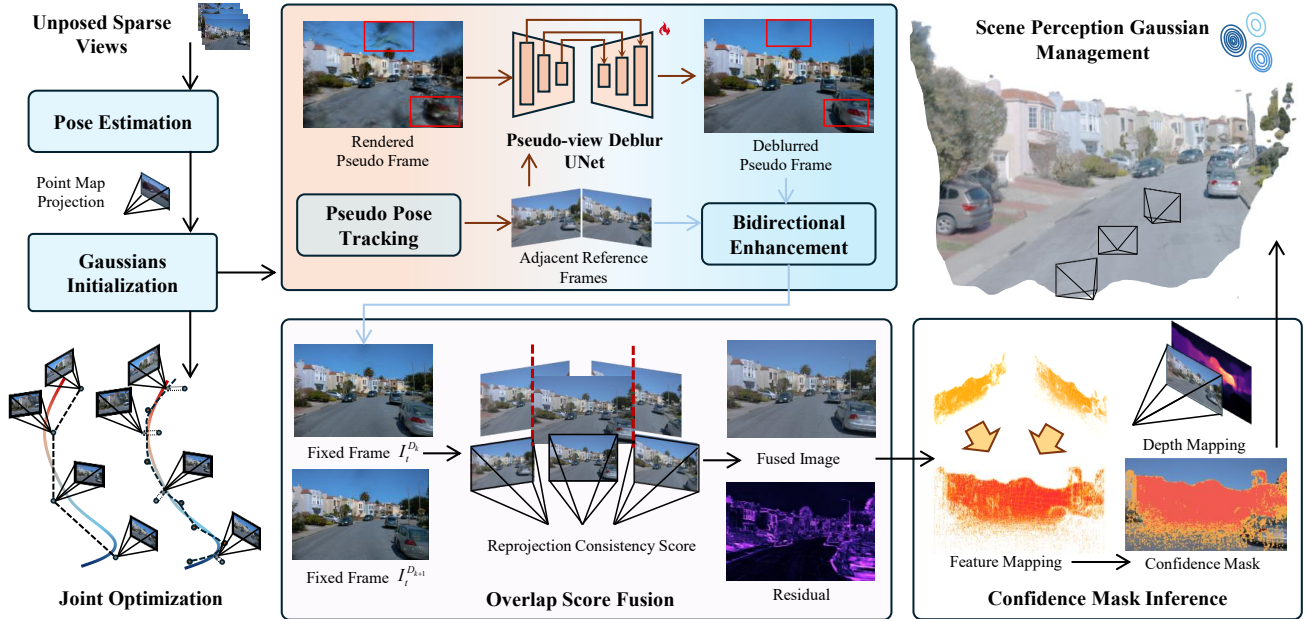


Figure 2. **Framework of BRPO.** We begin by the sparse input views and through the cross-view vision to select and restore frame. We design a lightweight pseudo-view deblur UNet to denoise the Gaussian rendered image and utilize a diffusion-based model for image completion. After that, we combine the two fixed images by calculating reprojection overlap score and conduct feature mapping to generate a confidence mask to guide the joint optimization.

2.2. 3D Gaussian Splatting from Sparse Views

Adequate view coverage is vital for high-quality novel view synthesis [13, 20, 40], while sparse input often causes floating artifacts and cross-view inconsistency. Some approaches [5, 15, 22, 32, 38, 41] integrate external geometric priors to enforce depth alignment. Others [18, 19, 31, 36, 42] use generative priors to regularize view-dependent effects. Complementary studies [11, 39] introduce opacity attenuation and binocular-guided photometric consistency to suppress floating artifacts and stabilize geometry. More recently, dropout and stochastic density modulation have been explored to improve robustness under sparse-view constraints [23, 33], while [1] explicitly mitigate co-adaptation effects. However, these methods typically need COLMAP priors or are limited to object-centric scenes.

RegGS [2] achieves unposed sparse-view reconstruction by registering locally generated Gaussian models from NoPoSplat [34] into a globally consistent representation, but only demonstrated on indoor scenes. Gscenes [24] develops a diffusion-driven, pose-free sparse-view pipeline that iteratively refines novel-view renders and depths with confidence-guided RGB-D priors, but its offline refinement and reliance on dense RGB-D supervision hinder scalability and efficiency. SGD [37] regularizes 3DGS for street scenes using diffusion prior conditioned on adjacent frames and LiDAR to improve sparse-view synthesis, but it assumes known poses and LiDAR supervision and remains scene-specific in its diffusion regularization.

We introduce a novel framework that tackles the challenge through bidirectional pseudo frame restoration and ensures robust optimization using a scene perception Gaussian management strategy, significantly enhancing reconstruction completeness and geometric consistency even under extreme view sparsity.

3. Methodology

Our framework aims to achieve high-quality outdoor 3D reconstruction under extremely sparse unposed viewpoints. The key idea is to augment the traditional pipeline with bidirectional pseudo frame restoration and scene perception Gaussian management. Specifically, we integrate four essential components: (1) a bidirectional pseudo frame restoration module with a pseudo-view deblur network for robust frame simulation, (2) a pseudo frame fusion algorithm for overlap score calculation and confidence mask inference, (3) a scene perception Gaussian management for Gaussians optimization, and (4) a joint optimization process coupling Gaussian attributes and camera poses. Fig. 2 illustrates the overall framework.

3.1. Bidirectional Pseudo Frame Restoration

Sparse camera sampling yields weak geometric constraints with missing detail and inconsistent appearance. Directly using these imperfect frames for Gaussian initialization or photometric alignment produces floating Gaussians and optimization instability. Therefore we first synthesize con-

sistent, perceptually faithful pseudo-frames that are used as reliable supervision for subsequent Gaussian construction and optimization. We propose a two-stage restoration pipeline for constructing reliable frames from sparse and possibly corrupted observations, which leverages geometric priors and reference information to enforce cross-view consistency during restoration process.

Pseudo-view Deblur Network. We observe that directly leveraging diffusion-based model for parse view completion will introduce unreasonable information which extremely harms and misleads the reconstruction quality. To better handle inter-frame inconsistencies and reduce artifacts before diffusion-based restoration, we introduce a lightweight pseudo-view deblur network U_c built on UNet backbone to integrate complementary cues from adjacent real frames while preserving the structure and color consistency of the current view.

Given the Gaussian-rendered current frame I_t^{gs} and its two neighboring reference frames I_k^{rf} and I_{k+1}^{rf} , the network predicts a refined image \hat{I}_t as:

$$\hat{I}_t = U_c \left(I_k^{\text{rf}}, I_t^{\text{gs}}, I_{k+1}^{\text{rf}} \right). \quad (1)$$

U_c employs a multi-scale UNet architecture with shared early encoders for reference alignment and skip connection for feature fusion. By modeling correlations between frames, the network explicitly compensates for viewpoint-induced inconsistencies, effectively removing ghosting and blending artifacts.

The refined output \hat{I}_t is then forwarded to the reference-conditioned diffusion model \mathcal{D} that produces two candidate restorations conditioned on the past and future references:

$$I_t^{D_k} = \mathcal{D}(\hat{I}_t, I_k^{\text{rf}}), I_t^{D_{k+1}} = \mathcal{D}(\hat{I}_t, I_{k+1}^{\text{rf}}), \quad (2)$$

which produces the final reliable frame from the fused representation.

Overlap Score Fusion. However, through different adjacent reference frames, the fixed image is different in details, which may be unreasonable. So we design a mixture algorithm to generate the final fixed frame. Given two cameras C_a and C_b , we first estimate their 2D overlap region by projecting the depth map of C_a into C_b :

$$\mathbf{p}_b = \Pi(\mathbf{K}, \mathbf{T}_b \mathbf{T}_a^{-1} \Pi^{-1}(\mathbf{p}_a, d_a)), \quad (3)$$

where p_a is a pixel in view a , Π and Π^{-1} denote projection and back-projection operators. The per-pixel overlap mask $O_{ab}(p)$ is defined by visibility consistency:

$$O_{ab}(p) = [\mathbf{p}_b \in \Omega_b] \wedge [d_b(\mathbf{p}_b) > \epsilon]. \quad (4)$$

The depth-consistency score s_d is:

$$s_d(p) = \exp\left(-\frac{|d_a(p) - d_b(\mathbf{p}_b)|}{(d_a(p) + d_b(\mathbf{p}_b))/2 + \epsilon}\right). \quad (5)$$

We further incorporate a pose-consistency scalar $s_t = \exp(-\|\mathbf{t}_a - \mathbf{t}_b\|_2)$ to down-weight references with large relative translation. We define the combined overlap confidence map:

$$\mathbf{C}_{ab}(p) = s_d(p) s_t. \quad (6)$$

Finally, we compute residuals $\mathbf{r}^{(i)} = \tilde{I}_t^{(i)} - I_t$ and form the fused repaired image:

$$I_t^{\text{fix}} = I_t + W_1 \odot \mathbf{r}^{(1)} + W_2 \odot \mathbf{r}^{(2)}, \quad (7)$$

where

$$W_i(p) = \frac{C_{t,i}(p)}{C_{t,1}(p) + C_{t,2}(p) + \epsilon}. \quad (8)$$

Confidence Mask Inference. While the fused pseudo-frame I_t^{fix} is visually enhanced, it may still contain geometric inconsistencies or ‘‘hallucinations’’ introduced by the diffusion model. Allowing this unstable information to propagate would degrade the final reconstruction quality. We therefore introduce a geometric verification step to generate a confidence map C_m , based on robust feature correspondences.

The core principle is that pixels in the synthetic frame I_t^{fix} must find geometrically consistent counterparts in the real reference frames. We leverage a robust correspondence network [14] to establish two mutual nearest-neighbor correspondence sets: (1) \mathcal{M}_k , linking I_t^{fix} and last reference I_k^{rf} , and (2) \mathcal{M}_{k+1} , linking I_t^{fix} and next reference I_{k+1}^{rf} .

Based on this bidirectional geometric constraint, we assign a confidence weight $C_m(p)$ to each pixel p in I_t^{fix} :

$$C_m(p) = \begin{cases} 1.0 & \text{if } p \in \mathcal{M}_k \cap \mathcal{M}_{k+1} \\ 0.5 & \text{if } p \in \mathcal{M}_k \oplus \mathcal{M}_{k+1} \\ 0.0 & \text{if } p \notin \mathcal{M}_k \cup \mathcal{M}_{k+1} \end{cases}. \quad (9)$$

This multi-level weighting strategy effectively suppresses artifacts by trusting only pixels with strong, bidirectionally-consistent geometric evidence, guiding the subsequent joint optimization.

3.2. Scene Perception Gaussian Management

Although the pseudo-views augment the input data, it is inadequate for the difficulty of joint optimization process. The optimization instability still corrupts the geometric integrity and visual fidelity, manifesting as floating artifacts and poorly-optimized Gaussians. We use scene perception Gaussian management that combines a 1D optimal-transport inspired depth partitioning with a global density-entropy driven adaptive scoring. The goal is to partition Gaussians adaptively and compute a stable per-Gaussian importance score that fuses depth and density cues.

Depth partitioning via 1D optimal transport. We treat the empirical distribution of depths $\{z_i\}$ as a one-dimensional probability measure on \mathbb{R}_+ . In one dimension, the p -Wasserstein distance admits a closed-form representation in terms of quantile functions (inverse CDF). For two probability measures μ, ν on \mathbb{R} with cumulative distribution functions F_μ, F_ν , the squared 2-Wasserstein distance is:

$$W_2^2(\mu, \nu) = \int_0^1 (F_\mu^{-1}(t) - F_\nu^{-1}(t))^2 dt. \quad (10)$$

This relationship implies that for 1D clustering of a single empirical measure into K contiguous clusters, quantile-based splits are a natural approximate minimizer of within-cluster Wasserstein energy because they align with the quantile geometry of the measure. Concretely, let F_N be the empirical CDF of depths and $Q_N(t) = F_N^{-1}(t)$ its quantile function. For $K = 3$ clusters we choose percentiles τ_1, τ_2 and define boundaries $b_1 = Q_N(\tau_1)$ and $b_2 = Q_N(\tau_2)$. The quantile choice yields contiguous depth intervals and approximates the minimization of intra-cluster Wasserstein cost in the 1D case. We get the depth score by:

$$\hat{s}_i^{(z)} = \frac{1 - d}{d_{\max} - d_{\min} + \delta}, \quad (11)$$

where d denotes the camera viewpoint depth.

Density entropy for global concentration. We next characterize the global structure of the density distribution $\{\rho_i\}$ using an information entropy measure. Distributions with low entropy are concentrated and high entropy indicates a more uniform density. We estimate a histogram-based discrete probability mass function from $\{\rho_i\}$. Let a histogram with B bins produce probabilities p_b , $b = 1, \dots, B$, with $\sum_b p_b = 1$. We normalize the Shannon entropy by the maximum achievable entropy $\log B$ to obtain:

$$H(\rho) = -\frac{1}{\log B} \sum_{b=1}^B p_b \log(p_b + \varepsilon), \quad (12)$$

where ε is a small constant for numerical stability. We then produce an entropy-aware fused density score $\hat{s}_i^{(\rho)}$:

$$\hat{s}_i^{(\rho)} = \tilde{\rho}_i \cdot (1 - \beta \bar{H}) + \bar{H} \cdot \gamma, \quad (13)$$

where $\beta, \gamma \in [0, 1]$ are hyperparameters (we use $\beta = 0.5$, $\gamma = 0.5$). This yields $\hat{s}_i^{(\rho)} \in [0, 1]$ and smoothly blends density and entropy priors. Finally, we combine depth and density into a unified importance score:

$$S_i = \alpha s_i^{(z)} + (1 - \alpha) \hat{s}_i^{(\rho)}, \quad (14)$$

where $\alpha \in [0, 1]$ balances depth vs. density. In our experiments we set $\alpha = 0.5$.

Cluster-aware drop probability. We design cluster-specific attenuation factors so that the pruning aggressiveness is tuned by depth. The drop probability is:

$$p_i^{\text{drop}} = r \cdot w_{\text{cluster}(i)} \cdot S_i, \quad (15)$$

where $w_{\text{cluster}(i)}$ denotes cluster weights designed for different depth levels divided by boundaries and r denotes initial drop-rate scalar. We sample and apply the binary mask:

$$\alpha_i \leftarrow \alpha_i \cdot m_i, \quad \text{where } m_i \sim \text{Bernoulli}(1 - p_i^{\text{drop}}). \quad (16)$$

This stochastic masking preserves a soft expectation of retained mass and empirically reduces deterministic boundary artifacts versus hard thresholding.

3.3. Joint optimization and Gaussian refinement

We adopt a two-stage optimization strategy: first stabilize poses and radiometric corrections, then jointly refine Gaussians and poses with geometric and appearance constraints.

Pose deltas and exposure stabilization. For early frames, we optimize pose offsets and exposure correction parameters while keeping the Gaussian collection mostly fixed. Concretely, for each viewpoint we parameterize pose updates as small rotation and translation deltas $\Delta \mathbf{R}_t$, $\Delta \mathbf{t}_t$ and per-view exposure parameters a_t, b_t that model a simple affine photometric correction:

$$I'_t = a_t I_t + b_t. \quad (17)$$

Early pose stabilization prevents errors from passing to Gaussian parameters, leading to drifting geometry. Joint optimization after stable pose initialization enforces tighter geometry-appearance coupling and more photorealistic reconstructions. During joint optimization, both the Gaussian parameters $\mathcal{G} = \{(\boldsymbol{\mu}_i, \boldsymbol{\Sigma}_i, \mathbf{c}_i, \alpha_i)\}$ and camera poses $\{\mathbf{T}_t\}$ are updated through a weighted RGB-D reconstruction loss:

$$\mathcal{L} = \beta \mathcal{L}_{\text{rgb}} + (1 - \beta) \mathcal{L}_d + \lambda_s \mathcal{L}_s, \quad (18)$$

where

$$\mathcal{L}_{\text{rgb}} = \frac{\|C_m \odot (I_t - \hat{I}_t)\|_1}{\|C_m\|_1}, \quad (19)$$

$$\mathcal{L}_d = \frac{\|C_m \odot (D_t - \hat{D}_t)\|_1}{\|C_m\|_1}. \quad (20)$$

Here, C_m is the confidence mask from Eq. 9, \mathcal{L}_s is a loss to regularize the scale of each Gaussian. The weight β (typically 0.95) balances the color and depth constraints. This stage jointly refines camera trajectories and the spatial–radiometric distribution of Gaussians.

Method	DL3DV [17]			Waymo [28]			KITTI [10]		
	PSNR↑	SSIM↑	LPIPS↓	PSNR↑	SSIM↑	LPIPS↓	PSNR↑	SSIM↑	LPIPS↓
CF-3DGS [9]	13.01	0.426	0.582	13.67	0.590	0.554	9.79	0.303	0.619
VideoLifter* [6]	17.84	0.519	0.433	13.53	0.471	0.592	8.356	0.194	0.647
Instantsplat [8]	10.88	0.351	0.615	12.49	0.564	0.645	9.926	0.367	0.654
Longsplat [16]	17.40	0.516	0.428	15.06	0.551	0.522	10.69	0.285	0.617
RegGS* [2]	19.77	0.612	0.391	-	-	-	-	-	-
OpenGS-SLAM [35]	16.08	0.428	0.403	21.37	0.765	0.457	13.87	0.433	0.537
S3PO-GS [4]	20.67	0.647	0.219	22.03	0.771	0.452	15.58	0.510	0.513
Ours	24.27	0.753	0.183	23.76	0.777	0.348	17.95	0.605	0.472

Table 1. **Novel View Synthesis Result on Three Dataset.** Note that some methods with a * means that this method fails to finish the reconstruction in some scenes due to the extremely sparse condition and we only shows the successful results.



Figure 3. **Visual quality on KITTI dataset.** Our approach consistently outperforms other models on different scenes, demonstrating advantages in challenging scenarios. Best viewed in color.

Gaussian Refinement. After pose convergence, we perform an appearance refinement of \mathcal{G} by minimizing

$$\mathcal{L}_{refine} = (1 - \lambda_{ssim}) \mathcal{L}_{L1} + \lambda_{ssim} (1 - \mathcal{L}_{SSIM}). \quad (21)$$

Here, both the \mathcal{L}_{L1} and \mathcal{L}_{SSIM} terms are also weighted by the confidence map C_m . This refinement encourages structural consistency and prevents over-expansion of Gaussian primitives, achieving photorealistic reconstruction.

4. Experiments

4.1. Experiments Setup

Datasets We evaluate the proposed method on three widely-used outdoor 3D reconstruction datasets that capture progressively more challenging imaging and viewpoint variation regimes.

- **DL3DV [17] (easy)**, a controlled outdoor benchmark with relatively dense multi-view coverage and moderate viewpoint changes. Scenes typically contain well-textured static geometry and limited occlusion.
- **Waymo [28] (moderate)**, a large-scale driving dataset with realistic city and highway scenes, varying lighting and moderately large inter-frame motion, which requires robustness to viewpoint shifts and partial occlusions while still providing sufficient correspondences for multi-view fusion.

- **KITTI [10] (hard)**, a driving dataset with extreme view-point changes, large motion parallax, and many regions with poor texture. Incorrectly appearance in poorly-constrained regions tends to produce severe artifacts.

Quantitative metrics reported in this paper include rendering quality measures (PSNR, SSIM and LPIPS) for novel view synthesis (NVS). For pose estimation evaluation, we use ATE RMSE as a metric. Detailed results are reported in the supplementary material.

Baselines. We compare our method with state-of-the-art methods for unposed reconstruction, including CF-3DGS [9], VideoLifter [6], Instantsplat [8], Longsplat [16], RegGS [2], OpenGS-SLAM [35] and S3PO-GS [4].

Implementation details. All experiments are implemented in PyTorch and run on one NVIDIA A6000 GPU. The diffusion backbone uses the publicly available Difx3D [31] pretrained weights as the initial generative prior for image-space correction. We utilize MAST3R [14] as the pose estimation model. We uniformly extract one-tenth of the frames from the KITTI and Waymo datasets as input, and extract one frame every 30 frames for the DL3DV dataset.

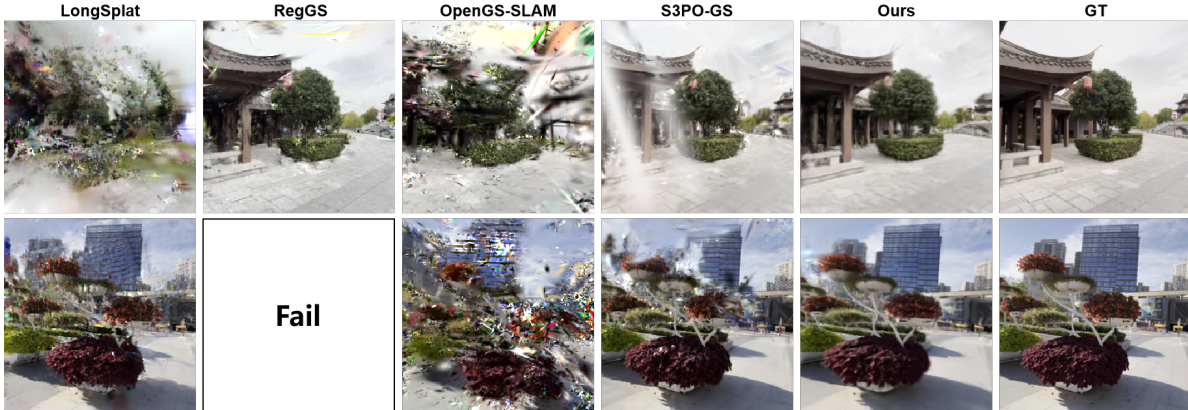


Figure 4. **Visual quality on DL3DV dataset.** Our approach consistently outperforms other models on different scenes, demonstrating advantages in challenging scenarios. Best viewed in color.

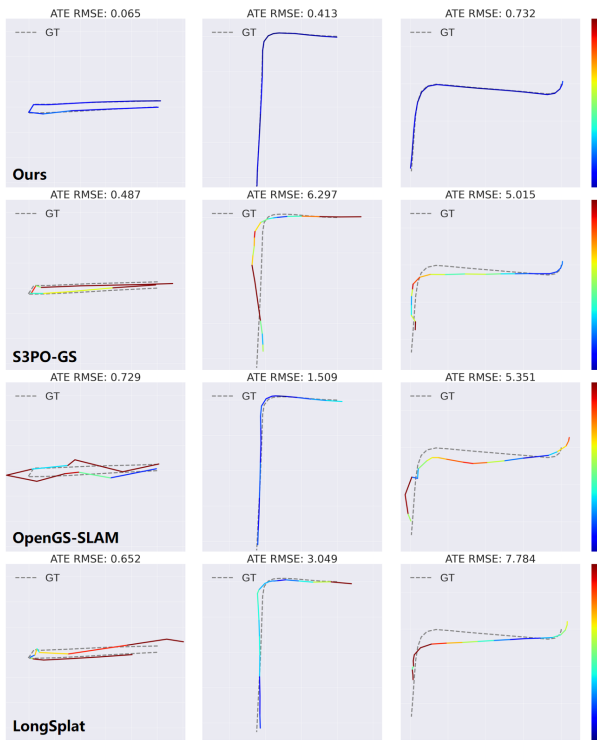


Figure 5. **Pose Estimation Visualization on KITTI and DL3DV dataset.** Our method can reach more accurate pose estimation compared to other methods.

4.2. Experimental Results and Analysis

In this section we present a focused analysis of the method’s performance across the three datasets as shown in Fig. 4, Fig. 3, Tab. 1 and Tab. 2. Across all datasets, we observe that the full pipeline consistently improves reconstruction fidelity and reduces view-dependent artifacts relative to baselines. On DL3DV the scene geometry is relatively well-

Method	DL3DV	Waymo	KITTI
CF-3DGS [9]	3.093	10.84	65.89
VideoLifter* [6]	3.184	32.71	81.22
Instantsplat [8]	0.333	9.992	65.10
Longsplat [16]	0.919	7.548	67.73
RegGS* [2]	2.045	-	-
OpenGS-SLAM [35]	1.586	1.784	4.722
S3PO-GS [4]	0.343	3.149	4.490
Ours	0.077	1.352	2.471

Table 2. **Pose Estimation Error–ATE RMSE on Three Dataset.**

constrained. We observe that in boundary regions, the diffusion model can introduce minor view-dependent inconsistencies. Our pseudo-view deblur module further improves quality by consolidating evidence from adjacent frames and suppressing these inconsistencies, while the confidence mask prevents over correction in predicted regions.

Waymo introduces tougher photometric variation and occlusions. The UNet effectively deblurs regions where single-view diffusion tends to inconsistent content. Gaussian optimization produces improvements by re-distributing gaussian weights to better match sparse view observations, which enables more accurate reprojected color priors.

KITTI is the most challenging dataset due to extreme viewpoint shifts and large textureless areas. The diffusion-only baseline tends to over-generate in texture-poor regions, producing plausible-looking but inconsistent appearance. The confidence mask is particularly important as it suppresses signals from reprojected pixels whose depth estimates are unreliable, preventing integrating misleading information. Although KITTI remains challenging, our method yields the largest relative improvements, demonstrating robustness in the face of severe viewpoint variation.

Method	Waymo-152706			KITTI-00		
	PSNR \uparrow	SSIM \uparrow	LPIPS \downarrow	PSNR \uparrow	SSIM \uparrow	LPIPS \downarrow
w/o Mask&Unet	19.76	0.735	0.440	13.63	0.527	0.508
w/o UNet	23.19	0.768	0.357	15.95	0.608	0.396
w/o Mask	24.40	0.779	0.385	16.90	0.638	0.395
w/o Bid-Fusion	24.29	0.776	0.378	17.13	0.636	0.379
w/o SPGM	24.03	0.774	0.381	17.10	0.628	0.382
w/o Depth	24.33	0.779	0.374	17.76	0.641	0.363
w/o Density	24.51	0.780	0.368	17.89	0.655	0.366
Ours	24.98	0.787	0.364	18.34	0.671	0.354

Table 3. Ablation Study on Waymo and KITTI.

4.3. Ablation Study

We conduct a series of controlled ablations to isolate the contribution of each component as shown in Tab. 3. Each ablation is evaluated on a held-out validation subset for each dataset. All other hyper-parameters and training schedules are kept identical across ablations.

w/o UNet & Mask. The diffusion prior often produces visually plausible completions, but in under-constrained regions it will “freely imagine” content that is inconsistent across views. This leads to large per-pixel and perceptual errors when the hallucinated content does not align with true geometry. Qualitatively, this appears as patchy or blurred seams when reprojected to other views.

w/o UNet. Introducing the UNet yields a significant reduction in these artifacts as shown in Fig. 6. Given the current Gaussian-rendered image and neighboring frames, the pseudo-view deblur UNet learns to keep reliable rendering information only where they are consistent with multi-view evidence and to suppress free hallucinations. This stage improves both pixel-wise metrics and perceptual consistency.

w/o Mask. When the UNet is allowed to fuse all reprojected information indiscriminately it can still be misled by reprojected pixels coming from unreliable depths or occlusions. The reprojection confidence mask gates the contribution of each reprojected sample. As shown in Fig. 7, using confidence mask to weight reprojected contributions yields an additional measurable improvement in both appearance and geometry metrics.

w/o Bid-Fusion. We validate the efficacy of bidirectional fusion. Compared to relies on information from only a single adjacent frame, the bidirectional mechanism demonstrates a clear advantage. By intelligently fusing features from multi reference frames, this bidirectional flow enables the compensation and averaging of potential errors inherent in any single view The result is a significant reduction in

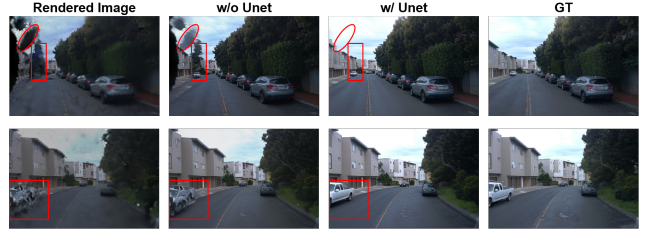


Figure 6. Ablation study on UNet The UNet can prefilter unreasonable artifacts and generate more reliable pseudo frame.

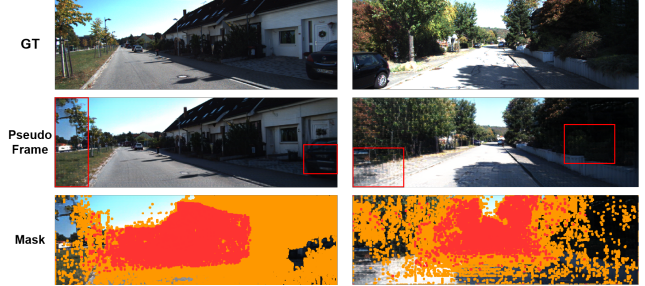


Figure 7. Ablation study on confidence mask The confidence mask can recognize unreliable regions in pseudo frames.

visual artifacts and a marked improvement in the geometric consistency of the restored regions.

w/o SPGM. We test the impact of the scene perception Gaussian management by disabling it while keeping all other components. Without this optimization, the reconstructions are less geometrically consistent and the diffusion stage contains noisier color priors, which results in a drop in geometry-aware metrics and a modest deterioration in appearance metrics. The results show that both depth and density regularization is vital for the reconstruction quality.

4.4. Limitations

While the proposed method demonstrates consistent improvements over strong baselines across a range of outdoor datasets, several limitations remain: Although our pipeline outperforms baselines on KITTI, scenes with extremely large viewpoint variation and large textureless regions still pose challenges. Diffusion priors may still introduce view-incoherent completions when multi-view constraints are insufficient. Improving robustness in these regimes will likely require stronger geometric priors. Our current framework assumes static scene geometry at the scale of fusion. Handling dynamics would require explicit motion modeling or temporal separation strategies.

5. Conclusion

This paper addresses the challenge of large-scale outdoor 3D scene reconstruction from extremely sparse views, a critical yet unsolved problem. We proposed a novel framework that combines bidirectional pseudo frame restoration with scene perception Gaussian management to overcome the limitations of existing methods in sparse, unposed outdoor settings. We introduce a lightweight pseudo-view deblur model to guide reliable pseudo-views generation and an overlap score fusion with confidence mask inference algorithm to fuse informative frames. Extensive experiments confirm that our method significantly improves reconstruction quality and visual consistency compared to state-of-the-art methods. Future work will extend the framework to 4D scenes.

Acknowledge

This work is supported by the National Natural Science Foundation of China (No. 62406267), Guangdong Provincial Project (No. 2024QN11X072), Guangzhou-HKUST(GZ) Joint Funding Program (No. 2025A03J3956) and Guangzhou Municipal Education Project (No. 2024312122).

References

- [1] Kangjie Chen, Yingji Zhong, Zhihao Li, Jiaqi Lin, Youyu Chen, Minghan Qin, and Haoqian Wang. Quantifying and alleviating co-adaptation in sparse-view 3d gaussian splatting. *arXiv preprint arXiv:2508.12720*, 2025. 3
- [2] Chong Cheng, Yu Hu, Sicheng Yu, Beizhen Zhao, Zijian Wang, and Hao Wang. Reggs: Unposed sparse views gaussian splatting with 3dgs registration. In *Proceedings of the IEEE/CVF International Conference on Computer Vision*, pages 8100–8109, 2025. 2, 3, 6, 7
- [3] Chong Cheng, Zijian Wang, Sicheng Yu, Yu Hu, Nanjie Yao, and Hao Wang. Unposed 3dgs reconstruction with probabilistic procrustes mapping. *arXiv preprint arXiv:2507.18541*, 2025. 2
- [4] Chong Cheng, Sicheng Yu, Zijian Wang, Yifan Zhou, and Hao Wang. Outdoor monocular slam with global scale-consistent 3d gaussian pointmaps. In *Proceedings of the IEEE/CVF International Conference on Computer Vision*, pages 26035–26044, 2025. 2, 6, 7
- [5] Jaeyoung Chung, Jeongtaek Oh, and Kyoung Mu Lee. Depth-regularized optimization for 3d gaussian splatting in few-shot images. In *Proceedings of the IEEE/CVF Conference on Computer Vision and Pattern Recognition*, pages 811–820, 2024. 3
- [6] Wenyan Cong, Hanqing Zhu, Kevin Wang, Jiahui Lei, Colton Stearns, Yuanhao Cai, Dilin Wang, Rakesh Ranjan, Matt Feiszli, Leonidas Guibas, et al. Videolifter: Lifting videos to 3d with fast hierarchical stereo alignment. *arXiv preprint arXiv:2501.01949*, 2025. 6, 7
- [7] Zhen-Hui Dong, Sheng Ye, Yu-Hui Wen, Nannan Li, and Yong-Jin Liu. Towards better robustness: Progressively joint pose-3dgs learning for arbitrarily long videos. *arXiv e-prints*, pages arXiv–2501, 2025. 2
- [8] Zhiwen Fan, Wenyan Cong, Kairun Wen, Kevin Wang, Jian Zhang, Xinghao Ding, Danfei Xu, Boris Ivanovic, Marco Pavone, Georgios Pavlakos, et al. Instantsplat: Sparse-view gaussian splatting in seconds. *arXiv preprint arXiv:2403.20309*, 2024. 2, 6, 7
- [9] Yang Fu, Sifei Liu, Amey Kulkarni, Jan Kautz, Alexei A Efros, and Xiaolong Wang. Colmap-free 3d gaussian splatting. In *Proceedings of the IEEE/CVF Conference on Computer Vision and Pattern Recognition*, pages 20796–20805, 2024. 2, 6, 7
- [10] Andreas Geiger, Philip Lenz, Christoph Stiller, and Raquel Urtasun. Vision meets robotics: The kitti dataset. *The international journal of robotics research*, 32(11):1231–1237, 2013. 6
- [11] Liang Han, Junsheng Zhou, Yu-Shen Liu, and Zhizhong Han. Binocular-guided 3d gaussian splatting with view consistency for sparse view synthesis. *Advances in Neural Information Processing Systems*, 37:68595–68621, 2024. 3
- [12] Kaiwen Jiang, Yang Fu, Mukund Varma T, Yash Belhe, Xiaolong Wang, Hao Su, and Ravi Ramamoorthi. A construct-optimize approach to sparse view synthesis without camera pose. In *ACM SIGGRAPH 2024 Conference Papers*, pages 1–11, 2024. 2
- [13] Bernhard Kerbl, Georgios Kopanas, Thomas Leimkühler, and George Drettakis. 3d gaussian splatting for real-time radiance field rendering. *ACM Trans. Graph.*, 42(4):139–1, 2023. 2, 3
- [14] Vincent Leroy, Yohann Cabon, and Jérôme Revaud. Grounding image matching in 3d with mast3r. In *European Conference on Computer Vision*, pages 71–91. Springer, 2024. 2, 4, 6, 1
- [15] Jiahe Li, Jiawei Zhang, Xiao Bai, Jin Zheng, Xin Ning, Jun Zhou, and Lin Gu. Dngaussian: Optimizing sparse-view 3d gaussian radiance fields with global-local depth normalization. In *Proceedings of the IEEE/CVF conference on computer vision and pattern recognition*, pages 20775–20785, 2024. 2, 3
- [16] Chin-Yang Lin, Cheng Sun, Fu-En Yang, Min-Hung Chen, Yen-Yu Lin, and Yu-Lun Liu. Longspat: Robust unposed 3d gaussian splatting for casual long videos. In *Proceedings of the IEEE/CVF International Conference on Computer Vision*, pages 27412–27422, 2025. 2, 6, 7
- [17] Lu Ling, Yichen Sheng, Zhi Tu, Wentian Zhao, Cheng Xin, Kun Wan, Lantao Yu, Qianyu Guo, Zixun Yu, Yawen Lu, et al. D13dv-10k: A large-scale scene dataset for deep learning-based 3d vision. In *Proceedings of the IEEE/CVF Conference on Computer Vision and Pattern Recognition*, pages 22160–22169, 2024. 6
- [18] Fangfu Liu, Wenqiang Sun, Hanyang Wang, Yikai Wang, Haowen Sun, Junliang Ye, Jun Zhang, and Yueqi Duan. Reconx: Reconstruct any scene from sparse views with video diffusion model. *arXiv preprint arXiv:2408.16767*, 2024. 3
- [19] Xi Liu, Chaoyi Zhou, and Siyu Huang. 3dgs-enhancer: Enhancing unbounded 3d gaussian splatting with view-

- consistent 2d diffusion priors. *Advances in Neural Information Processing Systems*, 37:133305–133327, 2024. 2, 3
- [20] Tao Lu, Mulin Yu, Linning Xu, Yuanbo Xiangli, Limin Wang, Dahua Lin, and Bo Dai. Scaffold-gs: Structured 3d gaussians for view-adaptive rendering. In *Proceedings of the IEEE/CVF Conference on Computer Vision and Pattern Recognition*, pages 20654–20664, 2024. 3
- [21] Hidenobu Matsuki, Riku Murai, Paul HJ Kelly, and Andrew J Davison. Gaussian splatting slam. In *Proceedings of the IEEE/CVF Conference on Computer Vision and Pattern Recognition*, pages 18039–18048, 2024. 2
- [22] Avinash Paliwal, Wei Ye, Jinhui Xiong, Dmytro Kotovenko, Rakesh Ranjan, Vikas Chandra, and Nima Khademi Kalantari. Coherentgs: Sparse novel view synthesis with coherent 3d gaussians. In *European Conference on Computer Vision*, pages 19–37. Springer, 2024. 3
- [23] Hyunwoo Park, Gun Ryu, and Wonjun Kim. Dropgaussian: Structural regularization for sparse-view gaussian splatting. In *Proceedings of the Computer Vision and Pattern Recognition Conference*, pages 21600–21609, 2025. 3
- [24] Soumava Paul, Prakhhar Kaushik, and Alan Yuille. Gaussian scenes: Pose-free sparse-view scene reconstruction using depth-enhanced diffusion priors. *arXiv preprint arXiv:2411.15966*, 2024. 2, 3
- [25] Erik Sandström, Ganlin Zhang, Keisuke Tateno, Michael Oechsle, Michael Niemeyer, Youmin Zhang, Manthan Patel, Luc Van Gool, Martin Oswald, and Federico Tombari. Splat-slam: Globally optimized rgb-only slam with 3d gaussians. In *Proceedings of the Computer Vision and Pattern Recognition Conference*, pages 1680–1691, 2025. 2
- [26] Johannes L Schonberger and Jan-Michael Frahm. Structure-from-motion revisited. In *Proceedings of the IEEE conference on computer vision and pattern recognition*, pages 4104–4113, 2016. 2
- [27] Dongbo Shi, Shen Cao, Lubin Fan, Bojian Wu, Jinhui Guo, Renjie Chen, Ligang Liu, and Jieping Ye. Trackgs: Optimizing colmap-free 3d gaussian splatting with global track constraints. *arXiv preprint arXiv:2502.19800*, 2025. 2
- [28] Pei Sun, Henrik Kretschmar, Xerxes Dotiwalla, Aurelien Chouard, Vijaysai Patnaik, Paul Tsui, James Guo, Yin Zhou, Yuning Chai, Benjamin Caine, Vijay Vasudevan, Wei Han, Jiquan Ngiam, Hang Zhao, Aleksei Timofeev, Scott Ettinger, Maxim Krivokon, Amy Gao, Aditya Joshi, Yu Zhang, Jonathon Shlens, Zhifeng Chen, and Dragomir Anguelov. Scalability in perception for autonomous driving: Waymo open dataset. In *Proceedings of the IEEE/CVF Conference on Computer Vision and Pattern Recognition (CVPR)*, 2020. 6
- [29] Jianyuan Wang, Minghao Chen, Nikita Karaev, Andrea Vedaldi, Christian Rupprecht, and David Novotny. Vggt: Visual geometry grounded transformer. In *Proceedings of the Computer Vision and Pattern Recognition Conference*, pages 5294–5306, 2025. 2
- [30] Shuzhe Wang, Vincent Leroy, Yohann Cabon, Boris Chidlovskii, and Jerome Revaud. Dust3r: Geometric 3d vision made easy. In *Proceedings of the IEEE/CVF Conference on Computer Vision and Pattern Recognition*, pages 20697–20709, 2024. 2
- [31] Jay Zhangjie Wu, Yuxuan Zhang, Haithem Turki, Xuanchi Ren, Jun Gao, Mike Zheng Shou, Sanja Fidler, Zan Gojcic, and Huan Ling. Difix3d+: Improving 3d reconstructions with single-step diffusion models. In *Proceedings of the Computer Vision and Pattern Recognition Conference*, pages 26024–26035, 2025. 2, 3, 6, 1
- [32] Haofei Xu, Songyou Peng, Fangjinhua Wang, Hermann Blum, Daniel Barath, Andreas Geiger, and Marc Pollefeys. Depthspat: Connecting gaussian splatting and depth. In *Proceedings of the Computer Vision and Pattern Recognition Conference*, pages 16453–16463, 2025. 2, 3
- [33] Yexing Xu, Longguang Wang, Minglin Chen, Sheng Ao, Li Li, and Yulan Guo. Dropouts: Dropping out gaussians for better sparse-view rendering. In *Proceedings of the Computer Vision and Pattern Recognition Conference*, pages 701–710, 2025. 3
- [34] Botao Ye, Sifei Liu, Haofei Xu, Xueting Li, Marc Pollefeys, Ming-Hsuan Yang, and Songyou Peng. No pose, no problem: Surprisingly simple 3d gaussian splats from sparse unposed images. *arXiv preprint arXiv:2410.24207*, 2024. 3
- [35] Sicheng Yu, Chong Cheng, Yifan Zhou, Xiaojun Yang, and Hao Wang. Rgb-only gaussian splatting slam for unbounded outdoor scenes. *arXiv preprint arXiv:2502.15633*, 2025. 2, 6, 7
- [36] Wangbo Yu, Jinbo Xing, Li Yuan, Wenbo Hu, Xiaoyu Li, Zhipeng Huang, Xiangjun Gao, Tien-Tsin Wong, Ying Shan, and Yonghong Tian. Viewcrafter: Taming video diffusion models for high-fidelity novel view synthesis. *arXiv preprint arXiv:2409.02048*, 2024. 2, 3
- [37] Zhongrui Yu, Haoran Wang, Jinze Yang, Hanzhang Wang, Jiale Cao, Zhong Ji, and Mingming Sun. Sgd: Street view synthesis with gaussian splatting and diffusion prior. In *2025 IEEE/CVF Winter Conference on Applications of Computer Vision (WACV)*, pages 3812–3822. IEEE, 2025. 3
- [38] Chuanrui Zhang, Yingshuang Zou, Zhuoling Li, Minmin Yi, and Haoqian Wang. Transplat: Generalizable 3d gaussian splatting from sparse multi-view images with transformers. In *Proceedings of the AAAI Conference on Artificial Intelligence*, pages 9869–9877, 2025. 2, 3
- [39] Jiawei Zhang, Jiahe Li, Xiaohan Yu, Lei Huang, Lin Gu, Jin Zheng, and Xiao Bai. Cor-gs: sparse-view 3d gaussian splatting via co-regularization. In *European Conference on Computer Vision*, pages 335–352. Springer, 2024. 3
- [40] Beizhen Zhao, Yifan Zhou, Sicheng Yu, Zijian Wang, and Hao Wang. Wavelet-gs: 3d gaussian splatting with wavelet decomposition. In *Proceedings of the 33rd ACM International Conference on Multimedia*, pages 8616–8625, 2025. 3
- [41] Yulong Zheng, Zicheng Jiang, Shengfeng He, Yandu Sun, Junyu Dong, Huaidong Zhang, and Yong Du. Nexusgs: Sparse view synthesis with epipolar depth priors in 3d gaussian splatting. In *Proceedings of the Computer Vision and Pattern Recognition Conference*, pages 26800–26809, 2025. 2, 3
- [42] Yingji Zhong, Zhihao Li, Dave Zhenyu Chen, Lanqing Hong, and Dan Xu. Taming video diffusion prior with scene-grounding guidance for 3d gaussian splatting from sparse in-

puts. In *Proceedings of the Computer Vision and Pattern Recognition Conference*, pages 6133–6143, 2025. [3](#)

Pseudo-View Enhancement via Confidence Fusion for Unposed Sparse-View Reconstruction

Supplementary Material

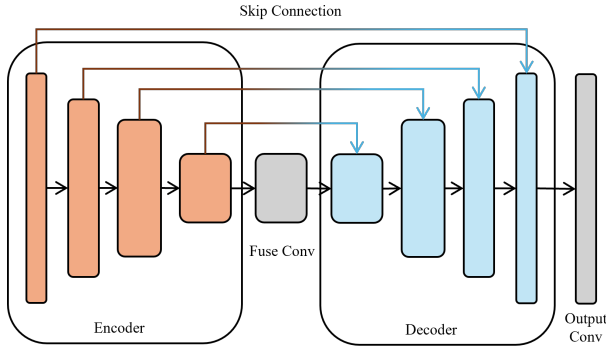


Figure 8. Structure of Pseudo-view Deblur UNet.

6. Training of Pseudo-view Deblur UNet

For the task of pseudo-view deblurring, we propose a novel lightweight UNet architecture. The detailed schematic of this network is illustrated in Fig. 8 and Fig. 9. The model is fundamentally based on a symmetric Encoder-Decoder (Enc-Dec) structure.

A critical design choice is the integration of skip connections, which bridge the corresponding layers between the encoder and decoder paths. These connections are essential for enhancing the network’s feature fusion capabilities. They allow the decoder to directly access low-level, high-resolution spatial information from the encoder, which is vital for reconstructing fine details and textures lost during the down-sampling process.

The lightweight UNet is trained entirely from scratch, without reliance on any pre-trained weights. To facilitate this, we generated a comprehensive synthetic dataset. This dataset contains over 10,000 image pairs, each consisting of rendered Gaussian images (as the blurred input) and their corresponding randomly designed neighbor reference frames.

The training process was performed on a high-performance computing setup, utilizing four NVIDIA A6000 GPUs operating in parallel. We employed the AdamW optimizer for parameter updates, selected for its robustness in training deep networks. The learning rate was dynamically managed using a cosine learning rate scheduler that included an initial warm-up mechanism to ensure stable convergence. The model was trained for 1000 epochs, achieving convergence in approximately 10 hours on this 4-A6000 configuration.

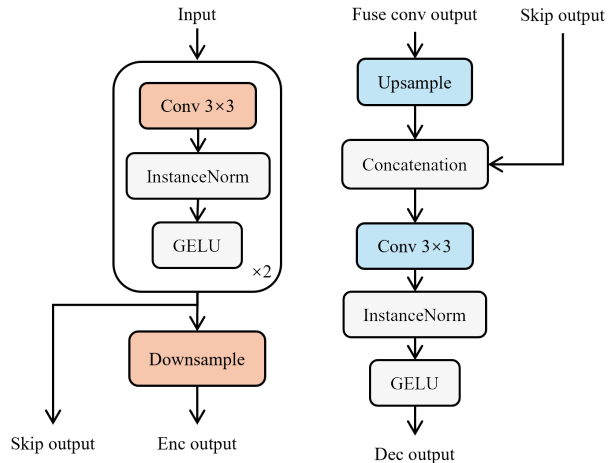


Figure 9. Detailed structure of Encoder (left) and Decoder (right).

Scene	1	2	3	Avg.
ATE	0.131	0.036	0.065	0.077
PSNR	27.34	22.70	22.78	24.27
SSIM	0.846	0.747	0.666	0.753
LPIPS	0.117	0.216	0.217	0.183

Table 4. Detailed results on DL3DV dataset.

7. More Experiment Results

All experiments are implemented in PyTorch and run on one NVIDIA A6000 GPU. The diffusion backbone uses the publicly available Difix3D [31] pretrained weights as the initial generative prior for image-space correction. We utilize Mast3R [14] as the pose estimation model. We uniformly extract one-tenth of the frames from the KITTI and Waymo datasets as input. Given that the DL3DV dataset is relatively dense and small, a sparser approach was necessary to prevent input redundancy. We therefore extracted only one frame every 30 frames from this dataset. For KITTI dataset, we choose the first 200 frames of each scenes. For Waymo dataset, we select the frame of front camera in nine scenes. Experimental ResultsThe detailed quantitative performance metrics across the evaluated datasets are systematically presented in the following tables: Tab. 4 (DL3DV dataset), Tab. 5 (Waymo dataset), and Tab. 6 (KITTI dataset).

Scene	100613	13476	106762	132384	152706	153495	158686	163453	405841	Avg.
ATE	0.719	1.567	1.022	1.465	2.257	2.530	1.154	0.834	0.621	1.352
PSNR	23.28	23.14	24.68	25.10	24.98	23.00	22.97	22.16	24.56	23.76
SSIM	0.779	0.712	0.821	0.855	0.787	0.757	0.746	0.742	0.796	0.777
LPIPS	0.314	0.440	0.272	0.261	0.364	0.354	0.381	0.382	0.365	0.348

Table 5. Detailed results on Waymo dataset.

Scene	00	02	03	05	06	07	08	10	Avg.
ATE	0.413	3.957	5.190	2.030	2.628	0.732	2.278	2.542	2.471
PSNR	18.34	17.39	19.16	18.07	18.18	17.82	18.09	16.53	17.95
SSIM	0.671	0.549	0.559	0.612	0.624	0.654	0.629	0.540	0.605
LPIPS	0.354	0.506	0.532	0.464	0.469	0.441	0.422	0.587	0.472

Table 6. Detailed results on KITTI dataset.



Figure 10. Visual quality on Waymo dataset. Our approach consistently outperforms other models on different scenes, demonstrating advantages in challenging scenarios. Best viewed in color.



Figure 11. **Visual quality on KITTI dataset.** Our approach consistently outperforms other models on different scenes, demonstrating advantages in challenging scenarios. Best viewed in color.



Figure 12. **Visual quality on DL3DV dataset.** Our approach consistently outperforms other models on different scenes, demonstrating advantages in challenging scenarios. Best viewed in color.



Figure 13. **Visual quality on Waymo dataset.** Our approach consistently outperforms other models on different scenes, demonstrating advantages in challenging scenarios. Best viewed in color.